Nonequilibrium Gas Flow and Heat Transfer in a Heated Square Microcavity

Giorgos Tatsios, Manuel H. Vargas, Stefan K. Stefanov & Dimitris Valougeorgis

Taylor & Francis
Taylor & Francis Group

Nonequilibrium Gas Flow and Heat Transfer in a Heated Square Microcavity

GIORGOS TATSIOS,[1] MANUEL H. VARGAS,[1] STEFAN K. STEFANOV,[2]
and DIMITRIS VALOUGEORGIS[1]

[1]Department of Mechanical Engineering, University of Thessaly, Volos, Greece
[2]Institute of Mechanics, Bulgarian Academy of Sciences, Sofia, Bulgaria

The flow of a rarefied gas in a square enclosure with one wall at high temperature and the other three walls at the same low temperature is investigated. The flow, characterized by the reference Knudsen number and ratio of the cold over the hot temperatures, is simulated both deterministically, using the nonlinear Shakhov kinetic model, and stochastically, using the DSMC method. Excellent agreement between the two approaches is obtained. It is found that along the side walls the gas velocity, depending on the flow parameters, may be either from cold to hot or from hot to cold regions. Furthermore, it is confirmed that the average heat flux departing from the hot plate exhibits a nonmonotonic behavior with regard to the temperature ratio, deducing a maximum heat flux at a temperature ratio of about 0.3. The flow and heat transfer characteristics are explained by computing the ballistic and collision parts of the total bulk quantities and by investigating the contribution of each part to the overall solution.

INTRODUCTION

Thermally driven rarefied gas flows in microcavities have received a lot of attention lately due to their potential implementation in the emerging field of gaseous microfluidics. Typical examples include vacuum-packed microelectromechanical systems (MEMS) where investigation of the gas flow and heat transfer is needed to improve cooling efficiency [1, 2] as well as actuation and sensing in microsystems based on the enhanced Knudsen thermal forces due to the decreasing size [3, 4]. In addition, various grooved channel configurations have been examined in designing micropumps by optimizing thermal transpiration effects and are applied in the typical Knudsen pump [5–7]. Thermally driven rarefied gas flows in cavities are also commonly applied in benchmarking of novel numerical schemes [8–10] and in the investigation of nonequilibrium phenomena that arise in such flows. It has been found that the flow

in a square enclosure caused by a discontinuous wall temperature vanishes in the continuum limit in a nonuniform manner [11]. At the other end, interesting features of the macroscopic variables in a free molecular gas in bounded domains are given in references 12 and 13. More recently, in cavities with different wall temperatures an unexpected type of flow along the cavity walls driving from the hot towards the cold regions has been reported in a wide range of gas rarefaction [14, 15].

The main dimensionless parameter characterizing rarefied flows is the Knudsen number, denoted by Kn, which is the ratio of the mean free path over a characteristic length of the flow. Flows characterized by small Knudsen numbers, which are in the slip or early transition regimes can be modeled by the conventional Navier–Stokes–Fourier (NSF) analysis with the appropriate slip and jump boundary conditions [16], or with higher order continuum models [17]. At higher values of the Knudsen number, when the flow is in the transition and free molecular regimes, the NSF approach fails and a kinetic approach must be applied [18, 19].

Recently the thermally driven gas flow in a microcavity with one wall maintained at high temperature and the other three walls at the same low temperature has been investigated in

Address correspondence to Professor Dimitris Valougeorgis, Department of Mechanical Engineering, University of Thessaly, Volos 38334, Greece. E-mail: diva@uth.gr

Color versions of one or more of the figures in the article can be found online at www.tandfonline.com/uhte.

reference 20 based on the NSF equations with slip and jump boundary conditions and the regularized 13 moment (R13) equations [17]. The results have been compared with corresponding direct simulation Monte Carlo (DSMC) results clearly indicating the limitations of the NSF and the R13 approaches. For this specific configuration, the former one cannot capture typical flow patterns even in the slip regime, while the latter one gives satisfying results in the transition regime but only up to $Kn \leq 0.3$.

In the present work this microcavity flow configuration is simulated in a much wider range of the Knudsen number based on both the nonlinear Shakhov kinetic model and the DSMC method for various temperature ratios of the high wall temperature over the low temperature of the other three walls. The implemented methodologies are the same as the ones introduced in reference 15 for solving a slightly different thermally driven cavity flow where low and high temperatures are imposed at two opposite walls, while at the other two the temperature varies linearly between these high and low temperatures. Note, however, that new interesting findings related to the average heat flux removed from the hot wall in terms of the temperature ratio of the cold over the hot wall, not observed before, are reported in the present work for first time. Furthermore, the recently introduced decomposition approach in reference 15 is implemented to interpret this behavior.

The paper is structured as follows: The flow configuration is defined in the second section, while the deterministic (Shakhov model) and the stochastic (DSMC) approaches are formulated in the third and fourth sections, respectively. The results are presented in the fifth section, and finally, some concluding remarks are provided in the sixth section.

FLOW CONFIGURATION

A monatomic rarefied gas is contained in a two-dimensional enclosure with square cross section of side length W. The cross section of the enclosure and the origin of the coordinate system (x', y') are shown in Figure 1. In the z' direction the enclosure is considered as unbounded and end effects in that direction are neglected. One wall, namely, the bottom one, without loss of generality, is at temperature T_H, while the other three walls are kept at temperature T_C, with $T_C < T_H$. To avoid discontinuities at the two bottom corners, the temperature of the hot wall close to the two corners (5 % of the total length W) is linearly decreased from T_H to match the side-walls temperature T_C.

Due to thermal creep, a flow is expected near the side walls directed from cold to hot regions, and to ensure mass conservation a flow near the symmetry axis ($x' = 0$) is expected in the opposite direction. This would create two counterrotating vortices in the enclosure. It turns out that in addition to these vortices, even at small Knudsen numbers, two more vortices appear in the upper part of the enclosure, with a flow along the lateral walls from hot to cold regions [14, 15, 20]. All four vortices are shown in Figure 1, with the former ones denoted by
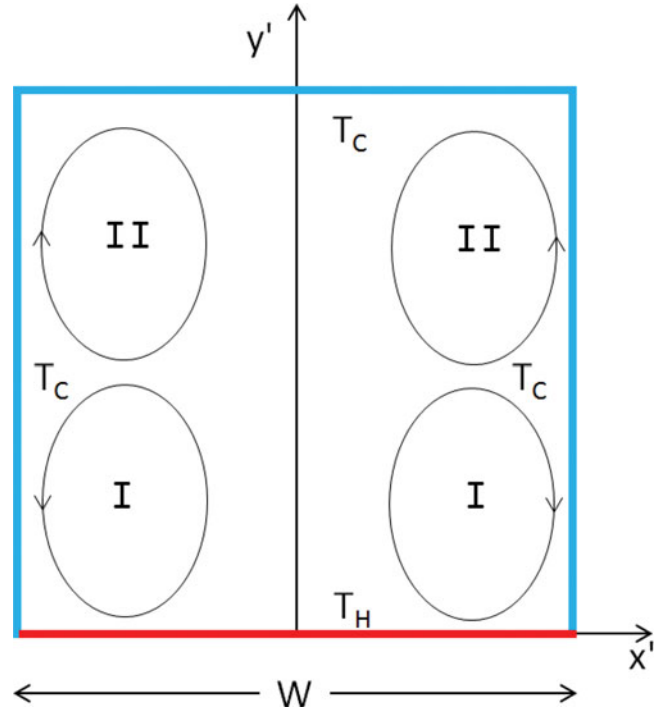

Figure 1 View of the bottom wall heated square cavity with the flow pattern of vortices I and II.

the symbol I and the latter unexpected ones by II. The detailed flow pattern depends on the gas rarefaction and the temperature ratio of the cold over the hot walls.

The two-dimensional macroscopic quantities of interest are the number density $N(x', y')$, the two-component velocity vector $U = [U_x(x', y'), U_y(x', y')]$, the temperature distribution $T(x', y')$, and the two-component heat flux vector $Q = [Q_x(x', y'), Q_y(x', y')]$, while the gas pressure is given by the ideal gas law $P = Nk_BT$, with k_B denoting the Boltzmann constant.

The problem is characterized by the reference Knudsen number, defined as

$$Kn_0 = \frac{\sqrt{\pi}}{2} \frac{\mu_0 \upsilon_0}{P_0 W} \tag{1}$$

and the temperature ratio T_C/T_H. In Eq. (1) P_0 is the reference pressure, W is the side length of the square cavity, μ_0 is the gas viscosity at reference temperature $T_0 = T_H$, and $\upsilon_0 = \sqrt{2k_BT_0/m}$ is the most probable molecular speed (m denotes the molecular mass). The reference number density $N_0 = \int_0^W \int_{-W/2}^{W/2} N dx' dy'$ is related to the reference pressure and temperature according to $P_0 = N_0 k_B T_0$.

The following dimensionless quantities are introduced:

$$x = x'/W, y = y'/W, n = N/N_0, u_x = U_x/\upsilon_0, u_y = U_y/\upsilon_0,$$

$$p = P/P_0, \tau = T/T_0, q_x = Q_x/(P_0\upsilon_0), q_y = Q_y/(P_0\upsilon_0) \tag{2}$$

The space variables are $x \in [-0.5, 0.5]$ and $y \in [0, 1]$, while $n, (u_x, u_y), p, \tau$, with $p = n \times \tau$ and (q_x, q_y), are the distributions of the number density, the two components of the velocity vector,

the gas pressure and temperature, and the two components of the heat flux vector, respectively. The hard sphere interaction is applied, yielding a viscosity of the form $\mu = \mu_0 \tau^{1/2}$, and purely diffuse gas–surface interaction is considered.

Another parameter of the flow field of practical interest is the local Mach number, defined as $Ma = |U/c_0|$, where $U = \sqrt{U_x^2 + U_y^2}$ is the magnitude of the bulk velocity and $c_0 = \sqrt{\gamma k_B T_0/m}$, with $\gamma = 5/3$ being the ratio of the specific heats of monatomic gases, is the speed of sound. It is readily shown that the local Mach number in terms of the dimensionless bulk velocity is given by $Ma = |u| \sqrt{6/5}$. The problem is solved both in a deterministic and stochastic manner. The deterministic modeling is based on the direct solution of the nonlinear Shakhov kinetic model [21, 22] and the stochastic modeling on the DSMC method [19].

DETERMINISTIC MODELING: THE SHAKHOV KINETIC MODEL

In kinetic modeling the main unknown is the distribution function, which for this flow configuration is a function of the two space variables and the three components of the molecular velocity vector, that is, $f = f(x, y, \xi_x, \xi_y, \xi_z)$. The flow is simulated by the nonlinear Shakhov kinetic model [21, 22]. It is noted that for this kinetic model the H-theorem has not been proved, and in addition to that, the positivity of the distribution function is not ensured. In spite of these pitfalls, the Shakhov model, also known as the S model, has been proved to be a reliable model for nonlinear heat transfer and non-isothermal flows [23–25], providing very good agreement with corresponding results of the solution of the Boltzmann equation and the DSMC method [26, 27].

The dimensionless distribution $g = f \upsilon_0^3/N_0$ and molecular velocities $\zeta = \xi/\upsilon_0$ along with the quantities of Eq. (2) are introduced into the model equation. Then the well-known projection procedure is applied to eliminate the z component of the molecular velocity by introducing the reduced distribution functions $\varphi = \int_{-\infty}^{\infty} g d\zeta_z$ and $\psi = \int_{-\infty}^{\infty} \zeta_z^2 g d\zeta_z$ and operating accordingly on the Shakhov equation yields the following system of integrodifferential equations [14]:

$$\zeta_x \frac{\partial \varphi}{\partial x} + \zeta_y \frac{\partial \varphi}{\partial y} = \frac{1}{Kn_0} \frac{\sqrt{\pi}}{2} n \sqrt{\tau} \left(\varphi^S - \varphi \right) \tag{3}$$

$$\zeta_x \frac{\partial \psi}{\partial x} + \zeta_y \frac{\partial \psi}{\partial y} = \frac{1}{Kn_0} \frac{\sqrt{\pi}}{2} n \sqrt{\tau} \left(\psi^S - \psi \right) \tag{4}$$

Here, the main unknowns are the reduced distribution functions $\varphi = \varphi(x, y, \zeta_x, \zeta_y)$ and $\psi = \psi(x, y, \zeta_x, \zeta_y)$, with ζ_x and ζ_y denoting the dimensionless x and y components of the molecular velocity vector; Kn_0 is defined by Eq. (1), while

$$\varphi^S = \varphi^M \left(1 + \frac{4}{15} \frac{1}{n\tau^2} \left[q_x \left(\zeta_x - u_x \right) + q_y \left(\zeta_y - u_y \right) \right] \right.$$

$$\times \left[\frac{\left(\zeta_x - u_x \right)^2 + \left(\zeta_y - u_y \right)^2}{\tau} - 2 \right] \right) \tag{5}$$

and

$$\psi^S = \psi^M \left(1 + \frac{4}{15} \frac{1}{n\tau^2} \left[q_x \left(\zeta_x - u_x \right) + q_y \left(\zeta_y - u_y \right) \right] \right.$$

$$\times \left[\frac{\left(\zeta_x - u_x \right)^2 + \left(\zeta_y - u_y \right)^2}{\tau} - 1 \right] \right) \tag{6}$$

with the reduced local Maxwellians given by

$$\varphi^M = \frac{n}{\pi \tau} \exp \left[-\frac{\left(\zeta_x - u_x \right)^2 + \left(\zeta_y - u_y \right)^2}{\tau} \right]$$

$$\psi^M = \frac{n}{2\pi} \exp \left[-\frac{\left(\zeta_x - u_x \right)^2 + \left(\zeta_y - u_y \right)^2}{\tau} \right] \tag{7}$$

By applying the same nondimensionalization and projection in the moments of the distribution function f, the macroscopic quantities in Eqs. (5)–(7) are readily deduced, and they are expressed in terms of φ and ψ according to the following double integrals:

$$n(x, y) = \int_{-\infty}^{\infty} \int_{-\infty}^{\infty} \varphi d\zeta_x d\zeta_y \tag{8}$$

$$u_x(x, y) = \frac{1}{n} \int_{-\infty}^{\infty} \int_{-\infty}^{\infty} \zeta_x \varphi d\zeta_x d\zeta_y \tag{9}$$

$$u_y(x, y) = \frac{1}{n} \int_{-\infty}^{\infty} \int_{-\infty}^{\infty} \zeta_y \varphi d\zeta_x d\zeta_y \tag{10}$$

$$\tau(x, y) = \frac{2}{3n} \int_{-\infty}^{\infty} \int_{-\infty}^{\infty} \left[\left(\zeta_x^2 + \zeta_y^2 \right) \varphi + \psi \right] d\zeta_x d\zeta_y$$

$$- \frac{2}{3} \left(u_x^2 + u_y^2 \right) \tag{11}$$

$$q_x(x, y) = \int_{-\infty}^{\infty} \int_{-\infty}^{\infty} \left[\left[\left(\zeta_x - u_x \right)^2 + \left(\zeta_y - u_y \right)^2 \right] \varphi + \psi \right]$$

$$\times \left(\zeta_x - u_x \right) d\zeta_x d\zeta_y \tag{12}$$

$$q_y(x, y) = \int_{-\infty}^{\infty} \int_{-\infty}^{\infty} \left[\left[\left(\zeta_x - u_x \right)^2 + \left(\zeta_y - u_y \right)^2 \right] \varphi + \psi \right]$$

$$\times \left(\zeta_y - u_y\right) d\zeta_x d\zeta_y \qquad (13)$$

The outgoing distributions at the boundaries are denoted by φ^+ and ψ^+ and are expressed by the Maxwell purely diffuse reflection as [15]

$$\varphi^+ = \frac{n_w}{\pi \tau_w} \exp\left[-\left(\zeta_x^2 + \zeta_y^2\right)/\tau_w\right]$$

$$\psi^+ = \frac{n_w}{2\pi} \exp\left[-\left(\zeta_x^2 + \zeta_y^2\right)/\tau_w\right] \qquad (14)$$

where τ_w is the dimensionless wall temperature and n_w is a parameter given in terms of the ingoing distributions satisfying the impermeability wall conditions.

The preceding set of integrodifferential equations (3) and (4) coupled with the expressions (5)–(13) subject to boundary conditions (14) is numerically solved using the discrete velocity method in the velocity space and a second-order control-volume scheme in the physical space. The implemented algorithm has been utilized to solve nonlinear non-isothermal flows and heat transfer problems with considerable success [15, 25, 28, 29]. Thus, here only some limited information on the computational approach is provided.

The molecular velocities ζ_x and ζ_y are transformed to polar coordinates, according to $\zeta_x = \zeta \cos\theta$ and $\zeta_y = \zeta \sin\theta$. Then the continuum velocity spectrum (ζ, θ) is replaced by a set of discrete velocities (ζ_m, θ_k), with $m = 1, 2, \ldots, M$ and $k = 1, 2, \ldots, K$. The magnitudes ζ_m are taken to be the roots of the Legendre polynomial of order M accordingly mapped from $(-1, 1)$ to $(0, +\infty)$, while the polar angles are $\theta_k = \pi (2k - 1)/K$. In the physical space the flow domain is divided into $I \times J$ rectangular elements, with $i = 1, 2, \ldots, I$ and $j = 1, 2, \ldots, J$.

Equations (3) and (4) are discretized in the molecular space and the deduced set of partial differential equations is solved by a typical second-order finite-volume scheme. The moments (8)–(13) are numerically integrated applying the trapezoidal rule in the polar angle θ and the Gauss–Legendre quadrature in the velocity magnitude ζ. The system of equations and their associated moments are solved in an iterative manner, which is terminated when the convergence criterion

$$\varepsilon^{(t)} = \max_{i,j} \left\{ \left| n_{i,j}^{(t)} - n_{i,j}^{(t-1)} \right| + \left| u_{xi,j}^{(t)} - u_{xi,j}^{(t-1)} \right| \right.$$

$$\left. + \left| u_{yi,j}^{(t)} - u_{yi,j}^{(t-1)} \right| + \left| \tau_{i,j}^{(t)} - \tau_{i,j}^{(t-1)} \right| \right\} \leq 10^{-13} \quad (15)$$

is fulfilled. Here, t denotes the iteration index and $\varepsilon^{(t)}$ the error after t iterations. Simulations have been performed with $I = J = 400$, $M = 80$, and $K = 400$. It may be useful to note that the implemented discrete velocity algorithm suffers a breakdown of the positivity of the distribution function, which is inherent in the Shakhov model. However, in all cases tested, the ratio of the weighted sums of the negative over the positive distributions is at least less than 10^{-4}, and therefore its effect on the implementation of the algorithm and the accuracy of the results is negligible. Upon convergence, all conservation principles are accordingly preserved and the results are accurate up to at least two significant figures.

STOCHASTIC MODELING: DSMC FORMULATION

The DSMC method [19] is based on splitting the real process of particle motion in two consecutive steps: (a) the collision between the particles, which is modeled in a stochastic manner within the particles at a given cell, and (b) the ballistic motion of the particles over a distance proportional to their velocities, which is purely deterministic. The standard No Time Counter (NTC) scheme [19], together with the HS molecular interaction model, is used for computing the collision between the particles. The interaction of the gas molecules with the solid walls is assumed to be purely diffuse.

Furthermore, following reference 15, the solution of the thermally induced flow in the enclosure is decomposed into the ballistic and collision parts. The ballistic part is due to particles arriving at this point from the boundaries of the flow domain with no collisions, while the collision part is due to particles arriving at this point after an arbitrary number of collisions (at least one). The decomposition of the particle distribution in a given cell of the computational grid is implemented by tagging with the indicator I_j all model particles $j = 1, \ldots, N_T$, where N_T is the total number of simulator particles. The indicator has the value of 0 or 1, indicating whether a particle contributes to the ballistic or the collision part of the distribution, respectively. A particle passes into the ballistic part when it is reflected from a wall and goes into the collision part when it interacts with another particle. The indicator is set to 0 each time that a particle is reflected from the bounding walls of the enclosure, while in the stage of particle free motion the indicators are not changed. In the stage of binary collisions the indicators (I_j, I_k) of any pair of particles (j, k) involved in a collision are set to 1. During the simulation process the particle indicators may change their values all the time. In the sampling stage of the macroscopic properties at given time t_k, all particles with indicators $I_j = 0$ are considered to belong to the ballistic part of the particle distribution and all particles with indicators $I_j = 1$ to the collision part. As a result, the total number of all particles accumulated in a cell is divided into two groups $N_T = N^{(b)} + N^{(c)}$, and the macroscopic quantities are sampled into the two corresponding parts.

Based on the preceding, the sampling of the ballistic and collision parts of the x components of the velocity and heat flux vectors is given by (the y components are computed in the same way by using the corresponding projections):

$$u_x^{(b)} = \frac{1}{N_T} \sum_{k=1}^{S} \sum_{i=1}^{N(t_k)} [1 - I_i(t_k)] \zeta_{x,i}(t_k),$$

$$u_x^{(c)} = \frac{1}{N_T} \sum_{k=1}^{S} \sum_{i=1}^{N(t_k)} I_i(t_k) \zeta_{x,i}(t_k). \tag{16}$$

$$\frac{q_x^{(b)}}{2} = \frac{1}{N_T} \sum_{k=1}^{S} \sum_{i=1}^{N(t_k)} [1 - I_i(t_k)] \zeta_{x,i} \left(\zeta_{x,i}^2 + \zeta_{y,i}^2 + \zeta_{z,i}^2 \right)$$

$$- u_x \left\{ \frac{1}{N_T} \sum_{k=1}^{S} \sum_{i=1}^{N(t_k)} [1 - I_i(t_k)] \left(\zeta_{x,i}^2 + \zeta_{y,i}^2 + \zeta_{z,i}^2 \right) \right\}$$

$$- 2u_x \left\{ \frac{1}{N_T} \sum_{k=1}^{S} \sum_{i=1}^{N(t_k)} [1 - I_i(t_k)] \zeta_{x,i}^2 \right\}$$

$$- 2u_y \left\{ \frac{1}{N_T} \sum_{k=1}^{S} \sum_{i=1}^{N(t_k)} [1 - I_i(t_k)] \zeta_{x,i} \zeta_{y,i} \right\}$$

$$+ \left(u_x^2 + u_y^2 + u_z^2 \right) \left(u_x^{(b)} - n^{(b)} u_x \right)$$

$$+ 2u_x(u_x u_x^{(b)} + u_y u_y^{(b)}). \tag{17}$$

$$\frac{q_x^{(c)}}{2} = \frac{1}{N_T} \sum_{k=1}^{S} \sum_{i=1}^{N(t_k)} I_i(t_k) \zeta_{x,i} \left(\zeta_{x,i}^2 + \zeta_{y,i}^2 + \zeta_{z,i}^2 \right)$$

$$- u_x \left\{ \frac{1}{N_T} \sum_{k=1}^{S} \sum_{i=1}^{N(t_k)} I_i(t_k) \left(\zeta_{x,i}^2 + \zeta_{y,i}^2 + \zeta_{z,i}^2 \right) \right\}$$

$$- 2u_x \left\{ \frac{1}{N_T} \sum_{k=1}^{S} \sum_{i=1}^{N(t_k)} I_i(t_k) \zeta_{x,i}^2 \right\}$$

$$- 2u_y \left\{ \frac{1}{N_T} \sum_{k=1}^{S} \sum_{i=1}^{N(t_k)} I_i(t_k) \zeta_{x,i} \zeta_{y,i} \right\}$$

$$+ \left(u_x^2 + u_y^2 + u_z^2 \right) \left(u_x^{(c)} - n^{(c)} u_x \right)$$

$$+ 2u_x(u_x u_x^{(c)} + u_y u_y^{(c)}). \tag{18}$$

Here, S denotes the number of samples, t_k indicates the different times over which the sampling is performed, and $N(t_k)$ is the number of particles in the cell at time t_k. The macroscopic properties are obtained by time averaging over $S = 5 \times 10^5$ time steps after the steady-state regime has been recovered. Note that number density, bulk velocity, and heat flux are equal to $n = n^{(b)} + n^{(c)}$, $u = u^{(b)} + u^{(c)}$, and $q = q^{(b)} + q^{(c)}$, respectively. This decomposition, which is described in a more detailed manner in reference15, is applied in the Results section of this paper to describe the behavior of the heat flux from the hot wall in terms of the imposed temperature ratio.

The space domain is discretized into 100×100 squared cells with size smaller than the mean free path, while the gas is represented by a discrete number of model particles. A total number of 10^6 model particles have been used and the time step was chosen to be about one-third of the cell traversal time $W/(n_C \upsilon_0)$, with n_C being the number of cells in the x direction. The sampling of the macroscopic quantities starts once the steady-state flow has been achieved, and is carried out by volume-based time averaging of the corresponding microscopic values of the particles at a given cell. These moments are accumulated over 10^5 time steps. This gives a sample size of approximately 10^7 particles per cell, which is sufficiently large to reduce the statistical scatter of the macroscopic results.

RESULTS AND DISCUSSION

The flow in the square cavity was simulated in a wide range of the Knudsen number, namely, for $0.1 \leq Kn_0 \leq 10^2$, and various temperature ratios $0.05 \leq T_C/T_H \leq 0.9$. Simulations have been conducted both by the deterministic and stochastic methods, and a very good agreement between corresponding results has been obtained.

In Figure 2 a view of the flow field in terms of the involved parameters is provided. The streamlines and the temperature contours are plotted for $Kn_0 = [0.1, 1, 10]$ and $T_C/T_H = [0.1, 0.9]$. At $Kn_0 = 0.1$ and for both temperature ratios the largest part of the cavity is covered by the typical thermal creep type vortices I, and vortices II are restricted near the side walls of the cavity. As the gas rarefaction is increased, vortices II start to expand squeezing the vortices I toward the bottom part of the cavity. As seen at $Kn_0 = 1$, vortices II are already well developed, covering large areas of the square cavity. The flow configuration is similar at $Kn_0 = 10$, with vortices I further squeezed toward the bottom of the cavity. These observations are valid for both temperature ratios $T_C/T_H = 0.1$ and 0.9, corresponding to large and small temperature differences, respectively, while in general at the same Kn_0 the dependency of the flow pattern on the temperature ratio T_C/T_H is qualitatively weak. In all the cases tested, the vertical velocity along the lateral walls is positive for the biggest part of the wall, leading to a flow directed from hot to cold regions.

The agreement between the Shakhov and corresponding DSMC results is very good, and this is demonstrated in Figures 3 and 4. In Figure 3, DSMC streamlines and temperature contours are plotted for $Kn_0 = 1$ and $T_C/T_H = 0.1$. In addition, in Figure 4 the computed temperatures based on the DSMC method and the Shakhov kinetic model along the axis $x = 0$ are plotted for various values of Kn_0 and T_C/T_H. It is seen that in all cases very good agreement is achieved.

The y component of the velocity distribution along the lateral walls $u_y(\mp 1/2, y)$ is shown in Figure 5. Due to symmetry, these results correspond to $x = \mp 1/2$. Results are provided with $T_C/T_H = [0.1, 0.5, 0.9]$ corresponding to large, moderate, and small temperature differences and in each case for
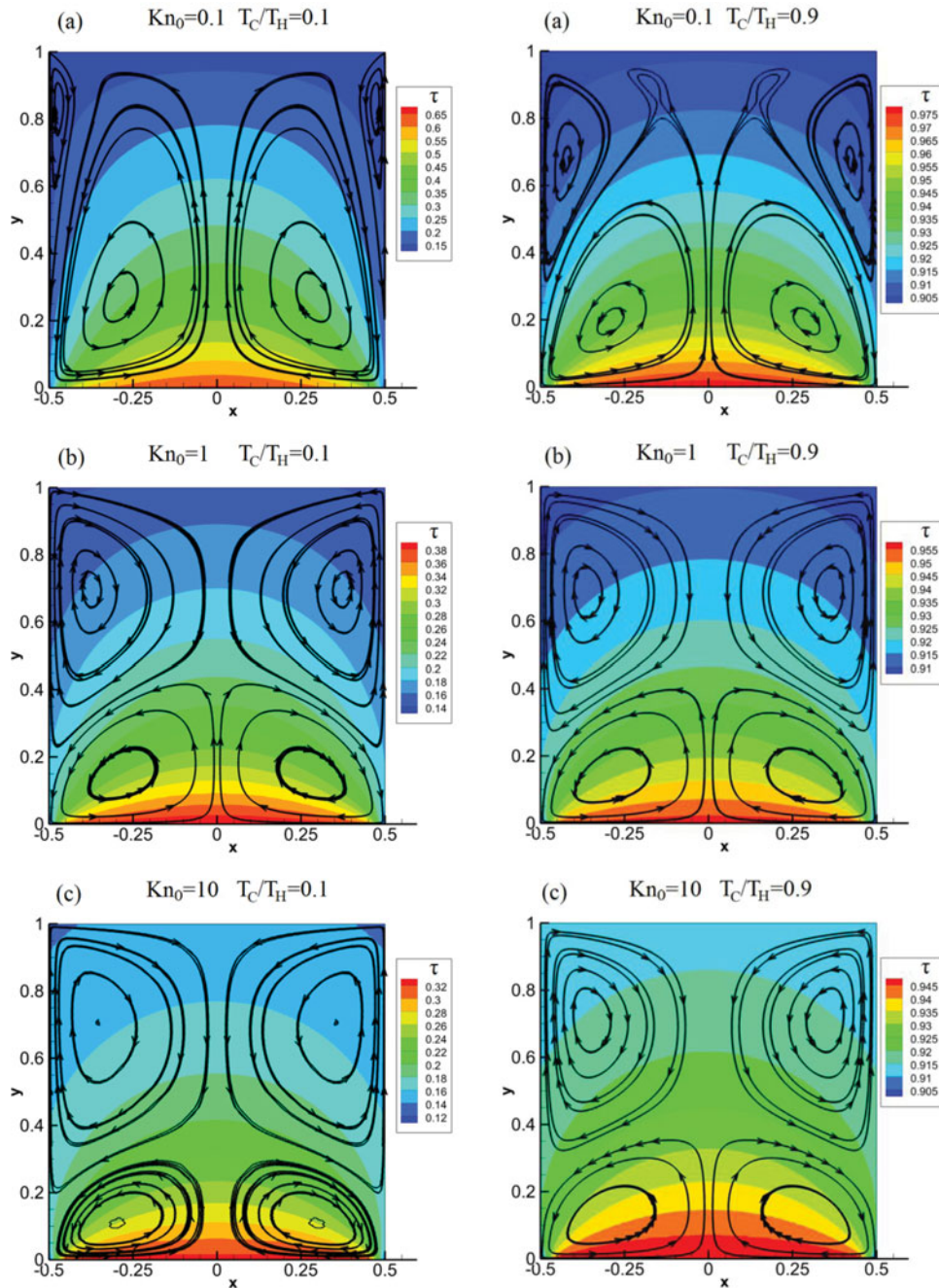
Figure 2   Streamlines and temperature contours for $T_C/T_H = 0.1$ (left) and $T_C/T_H = 0.9$ (right) for and various Knudsen numbers.

$Kn_0 = [0.1, 1, 10]$. The negative values of the velocity are related to the well-known thermal creep flow from cold to hot, whereas the positive ones relate to a nonequilibrium flow from hot to cold. We observe that even for small Knudsen numbers, and for all temperature ratios, in the biggest part of the two vertical walls the velocity is positive, leading to a mass flow rate from hot to cold. This type of flow has been explained when the flow is in the slip regime in [14, 20] and more recently in the whole range of the Knudsen number in reference 15, where the physical explanation is provided by splitting the flow

into a ballistic and collision part, as described in the DSMC section. It has been found in reference 15 that at very small Knudsen numbers the collision part is dominating and the classic thermal creep theory works well predicting the cold-to-hot flow along the vertical walls. As the Knudsen number increases, the impact of the ballistic part also increases and the convective vortices start to rotate in the hot-to-cold direction along the lateral walls. At these moderate Knudsen numbers there is interplay between the ballistic and collision parts, and the behavior of the overall solution is very subtle, particularly in
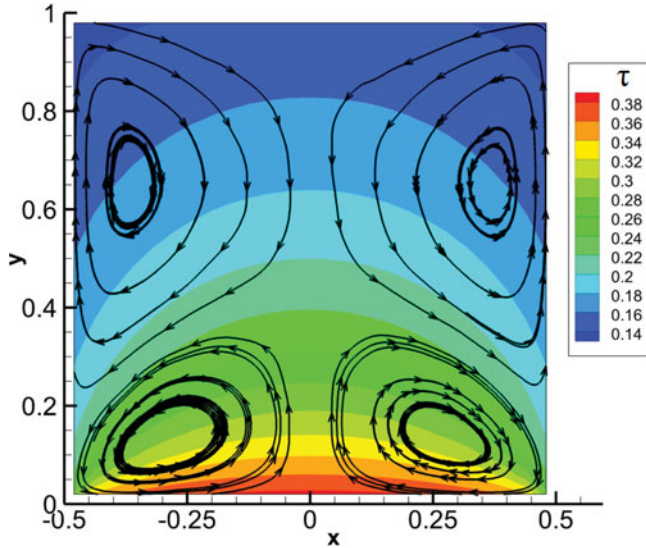
Figure 3 Streamlines and temperature contours for $Kn_0 = 1$ and $T_C/T_H = 0.1$ obtained by the DSMC method.

the transition regime. At large Knudsen numbers, the ballistic part and thus the hot-to-cold flow dominates, while of course as the Knudsen number tends to infinity the gas velocity vanishes. Exactly the same physical description explains the direction of the velocity streamlines in the present configuration. The decomposition methodology is extended in the present work to compute the ballistic and collision parts of the heat flux.

The local Mach number may be calculated based on the relation $Ma = |u| \sqrt{6/5}$, defined in the second section. To have some information for the velocity field, the maximum Mach number is tabulated in Table 1. It is seen that it is increased as the reference Knudsen number is decreased and the temperature difference between the hot and cold plates is increased. Also, in
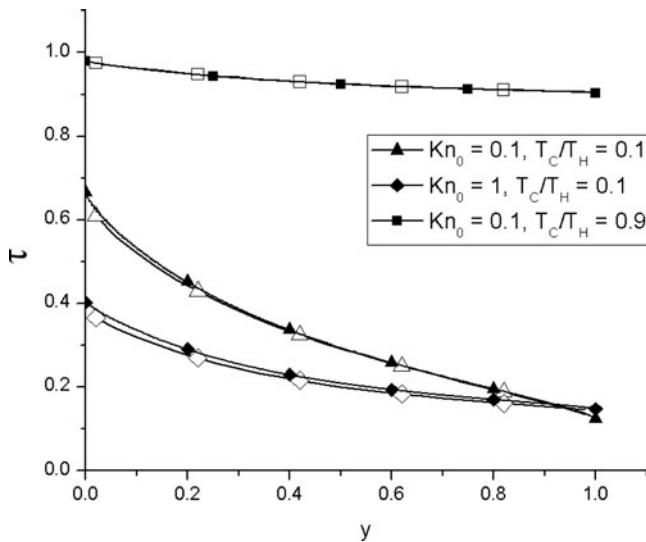

Figure 4 Temperature distribution along the axis $x = 0$ for various values of Kn_0 and T_C/T_H obtained by the DSMC method (open symbols) and the Shakhov kinetic model (filled symbols).
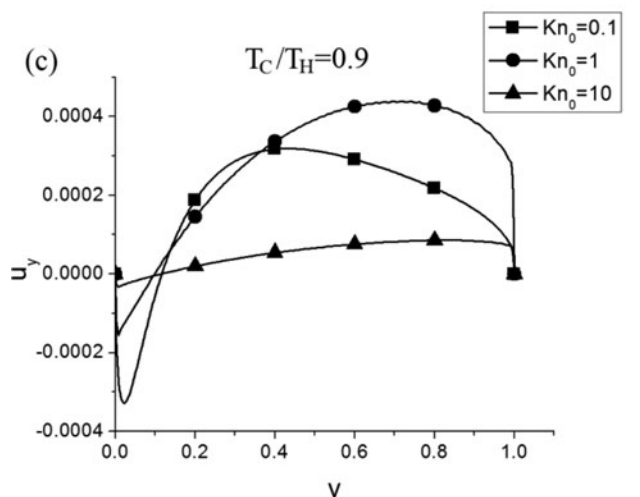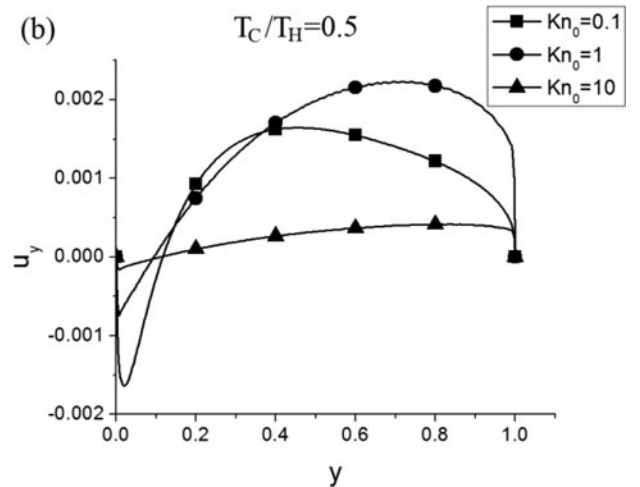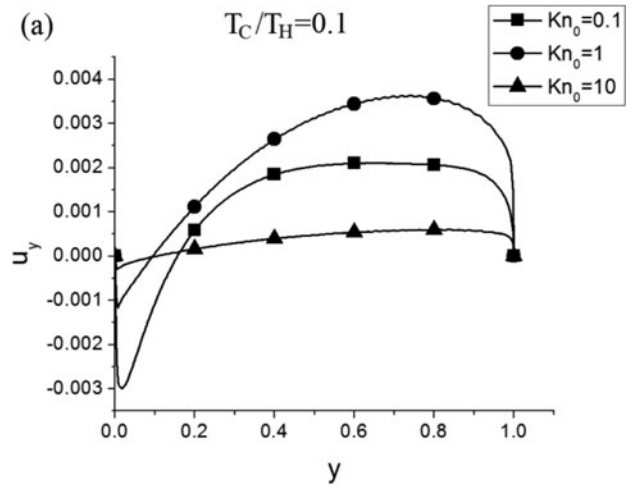

Figure 5 Distribution of the tangential velocity u_y ($\mp 1/2$, y) along the lateral walls of the cavity for various temperature ratios and Knudsen numbers.

Figure 6, typical contours of the Mach number are plotted for $Kn_0 = 1$ and $T_C/T_H = [0.1, 0.9]$. In general, as expected for flows induced by temperature differences, the Mach number is very small.

Table 1 Maximum value of the Mach number in the field for various Kn_0 and T_C/T_H

	Kn_0		
$\frac{T_C}{T_H}$	0.1	1	10
0.1	9.19 (–3)	3.99 (–3)	9.21 (–4)
0.5	3.69 (–3)	2.45 (–3)	4.62 (–4)
0.9	7.21 (–4)	4.83 (–4)	9.54 (–5)

Figure 7 Average heat flux q_{ave} departing from the hot plate of the cavity in terms of the Knudsen number for various temperature ratios.

An overall quantity of great practical interest for this specific heat flow configuration is the average dimensionless heat flux q_{ave} departing from the hot plate, which is estimated by integrating the heat flux $q_y(x, 0)$ over $x \in [-0.5, 0.5]$. This quantity is plotted in Figure 7 in terms of Kn_0 for various temperature ratios $T_C/T_H = [0.05, 0.1, 0.3, 0.5, 0.9]$. Results obtained both by the kinetic modeling and the DSMC approaches are provided for comparison purposes. As seen, the agreement is excellent in all cases. For all temperature ratios the average dimensionless heat flux increases as Kn_0 increases from 0.1 to 1 and then for $T_C/T_H = [0.3, 0.5, 0.9]$ keeps slowly increasing, while for $T_C/T_H = [0.05, 0.1]$ it is slightly decreasing. In all cases as $Kn_0 \to \infty$, q_{ave} tends to an asymptotic value. A very interesting result is the variation of q_{ave} in terms of T_C/T_H at a given Kn_0. It is clearly seen that q_{ave} is not steadily increased as the temperature difference between the hot and cold plates becomes greater, that is, as T_C/T_H is decreased. For example, at $Kn_0 = 1$, as the temperature ratio T_C/T_H is decreased from 0.9 to 0.3 the average heat flux is, as expected, increased, while as T_C/T_H is further decreased from 0.3 to 0.05 the average heat flux is decreased. This observation is valid in a whole range of the reference Knudsen number tested, and it is found that the maximum average heat flux emitted from the hot wall occurs at about $T_C/T_H = 0.3$. This behavior has been captured individually by both modeling approaches.

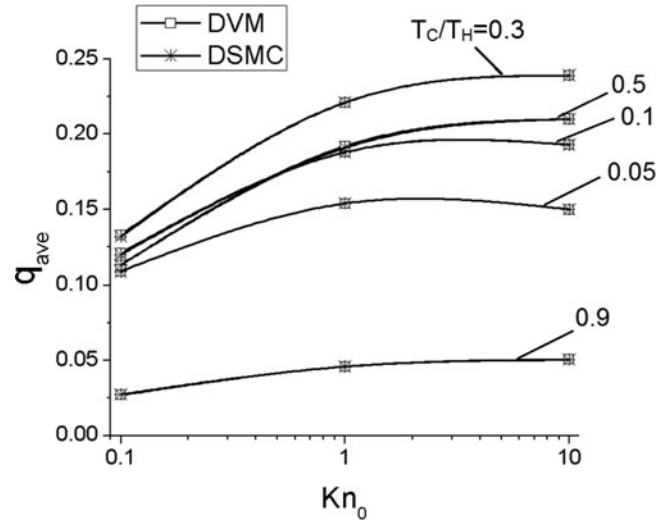To further investigate this finding, in Figure 8, the ballis-

tic and collision parts of the average heat flux at the hot wall, denoted as $q_{ave}^{(b)}$ and $q_{ave}^{(c)}$, respectively, are plotted in terms of the temperature ratio T_C/T_H for $Kn_0 = 1$. They have been computed according to Eqs. (17) and (18). The total average heat flux $q_{ave} = q_{ave}^{(b)} + q_{ave}^{(c)}$ is plotted as well. The ballistic and collision parts of the heat flux are opposed with $q_{ave}^{(b)} > 0$ and $q_{ave}^{(c)} < 0$, while their summation, that is, the total average heat flux, is always, as expected, larger than zero ($q_{ave} > 0$). It is seen that as T_C/T_H is increasing, initially $q_{ave}^{(b)}$ is increasing at a pace that is faster than the one with which $q_{ave}^{(c)}$ is decreasing, and therefore the total heat flux q_{ave} is initially increasing with T_C/T_H. Then, as T_C/T_H is further increasing, $q_{ave}^{(b)}$ is increasing at a slower pace, and finally, for large values of T_C/T_H it is even decreasing, while in parallel $q_{ave}^{(c)}$ always keeps increasing, and therefore after some critical value of T_C/T_H the total heat flux q_{ave} is decreasing. Consequently, the non-
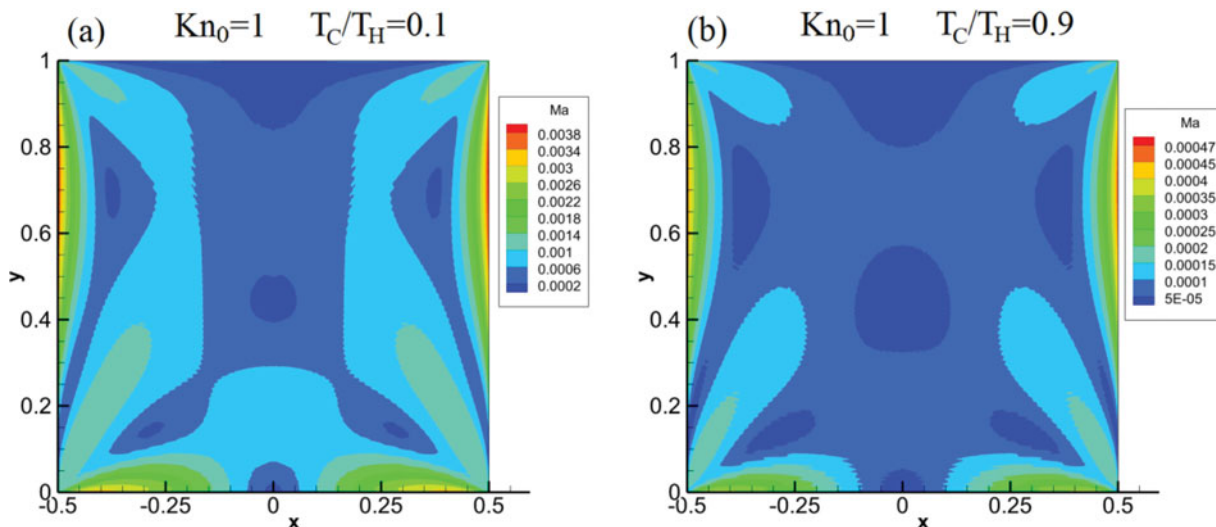

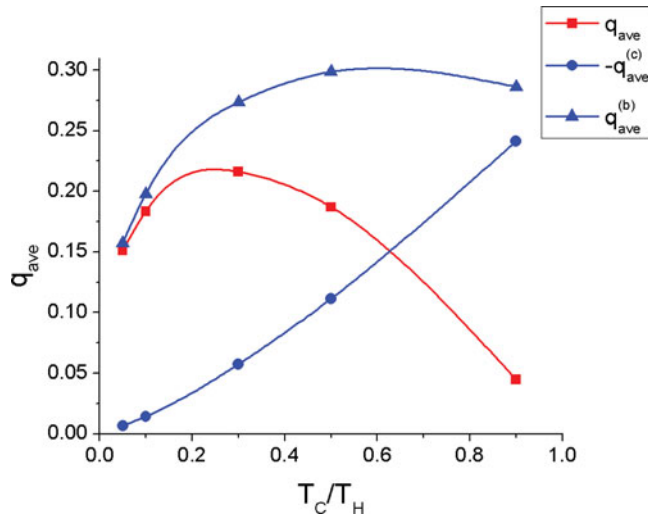**Figure 6** Typical contours of the Mach number in the flow field.

Figure 8 Average heat flux q_{ave} along with its ballistic and collision parts $q_{ave}^{(b)}$ and $q_{ave}^{(c)}$, respectively, departing from the hot plate of the cavity in terms of the temperature ratio for $Kn_0 = 1$.

monotonic behavior and the maximum q_{ave} at $T_C/T_H = 0.3$ may be explained by analyzing the overall solution to its ballistic and collision parts. Also, as $T_C/T_H \to 1$ the ballistic and collision parts have the same magnitude, and due to their opposite sign the total heat flux q_{ave} vanishes. The results are typical also for other values of the reference Knudsen number.

Some indicative dimensional results are shown in Figure 9, where the dimensional average heat flux Q_{ave} (W/m²) is plotted in terms of the reference pressure P_0 (Pa) for various values of $T_C/T_H = [0.05, 0.1, 0.3, 0.5, 0.9]$. The results are for a square cavity with a side length of $W = 50$ μm and the hot wall temperature equal to $T_H = 10^3$ K filled with argon
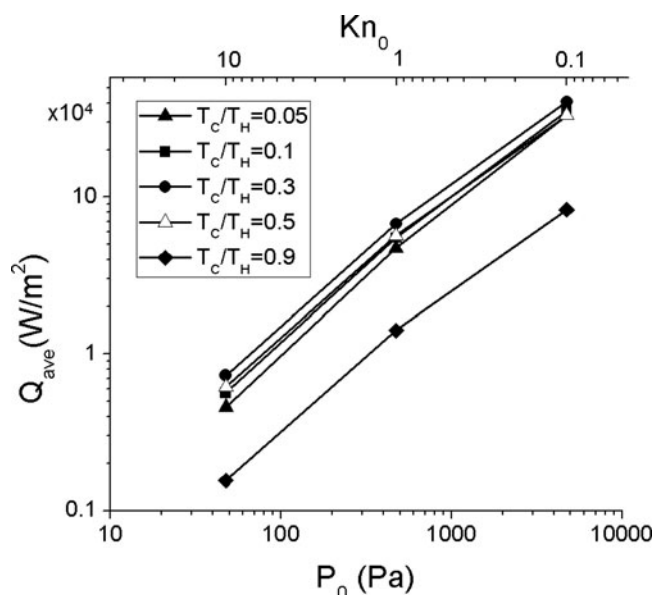
$(m = 39.95$ kg/kmol). The dimensional Q_{ave} is easily deduced from the corresponding dimensionless one via Eq. (2). The corresponding Kn_0 is also shown in Figure 9. It is seen that Q_{ave} is steadily increased as P_0 is increased, that is, as the gas becomes less rarefied. It is also seen that for the same P_0, as T_C/T_H is decreased from 0.9 to 0.3, Q_{ave} is increased, and then as T_C/T_H is further decreased to 0.1, Q_{ave} is decreased. Thus, as in the dimensionless results, there is a maximum value of Q_{ave} at $T_C/T_H = 0.3$. It may be stated that in order to maximize cooling a temperature ratio close to 0.3 is to be used, while to optimize operation stability (and probably efficiency) a temperature ratio close to $0.1 - 0.4$, depending on Kn_0, can be used.

CONCLUDING REMARKS

The nonequilibrium gas flow and heat transfer in a two-dimensional square cavity with one wall maintained at high temperature T_H and the other three at low temperature T_C has been numerically investigated. Simulations have been conducted for the two parameters characterizing the problem, namely, the temperature ratio T_C/T_H and the reference Knudsen number Kn_0, based on the Shakhov kinetic model and the DSMC method, deducing excellent agreement between the two methodologies.

It has been found that the flow along the lateral walls is directed form hot to cold even for small temperature differences and small Knudsen numbers, confirming previous findings in similar setups [14, 15, 20]. As the temperature difference and the Knudsen number are increased, this nonequilibrium flow pattern becomes more dominant. Also, the average heat flux departing from the hot plate exhibits a nonmonotonic dependency with regard to the temperature ratio T_C/T_H over a wide range of Kn_0. More specifically, a maximum heat flux occurs at $T_C/T_H = 0.3$. This behavior is explained by computing the ballistic and collision parts of the total heat flux and by investigating the contribution of each part to the overall solution. Overall, it is believed that this work has both scientific and technological interest since such flows are very common in various gaseous microdevices.

Figure 9 Average heat flux Q_{ave}(W/m²) departing from the hot plate of the cavity in terms of reference pressure for various temperature ratios.

NOMENCLATURE

c_0	speed of sound (m/s)
f	distribution function (particles/m⁶ s⁻³)
g	dimensionless distribution function

k_B Boltzmann's constant (J/K)

Kn Knudsen number

m molecular mass (kg/kmol)

Ma Mach number

N number density (particles/m^3)

n dimensionless number density

N_T total number of simulator particles for the DSMC method

n_w parameter

P pressure (Pa)

p dimensionless pressure

$\boldsymbol{Q}$ heat flux vector (W/m^2)

$\boldsymbol{q}$ dimensionless heat flux vector

Q_{ave} average heat flux departing from the bottom plate (W/m^2)

q_{ave} average dimensionless heat flux departing from the bottom plate

S number of samples for the DSMC method

T temperature (K)

$\boldsymbol{U}$ velocity vector (m/s)

$\boldsymbol{u}$ dimensionless velocity vector

W side length (m)

x',y',z' coordinates (m)

x,y,z dimensionless coordinates

Greek Symbols

γ specific heat of monatomic gases

ζ dimensionless molecular velocity vector

ζ dimensionless molecular velocity magnitude

θ polar angle of molecular velocity

μ viscosity (Pa-s)

ξ molecular velocity vector (m/s)

τ dimensionless temperature

υ_0 most probable molecular speed (m/s)

φ reduced distribution function

φ^M reduced Maxwellian

φ^S reduced equilibrium distribution function

φ^+ outgoing reduced distribution function

ψ reduced distribution function

ψ^M reduced Maxwellian

ψ^S reduced equilibrium distribution function

ψ^+ outgoing reduced distribution function

Superscripts

(b) ballistic part of macroscopic property

(c) collision part of macroscopic property

REFERENCES

[1] Yang, H. A., Wu, M. C., and Fang, W. L., Localized Induction Heating Solder Bonding for Wafer Level MEMS Packaging, *Journal of Micromechanics and Microengineering*, vol. 15, no. 2, pp. 394–399, 2005.

[2] Liu, H., Wang, M., Wang, J., Zhang, G., Liao, H., Huang, R., and Zhang, X., Monte Carlo Simulations of Gas Flow and Heat Transfer in Vacuum Packaged MEMS Devices, *Applied Thermal Engineering*, vol. 27, no. 2–3, pp. 323–329, 2007.

[3] Ketsdever, A., Gimelshein, N., Gimelshein, S., and Selden, N., Radiometric Phenomena: From the 19th to the 21st Century, *Vacuum*, vol. 86, no. 11, pp. 1644–1662, 2012.

[4] Vargas, M., Wüest, M., and Stefanov, S., Monte Carlo Analysis of Thermal Transpiration Effects in Capacitance Diaphragm Gauges With Helicoidal Baffle System, *Journal of Physics: Conference Series*, vol. 362, p. 012013, 2012.

[5] Sone, Y., Waniguchi, Y., and Aoki, K., One-Way Flow of a Rarefied Gas Induced in a Channel With a Periodic Temperature Distribution, *Physics of Fluids*, vol. 8, no. 8, pp. 2227–2235, 1996.

[6] Alexeenko, A., Gimelshein, S., Muntz, E., and Ketsdever, A., Kinetic Modeling of Temperature Driven Flows in Short Microchannels, *International Journal of Thermal Sciences*, vol. 45, no. 11, pp. 1045–1051, 2006.

[7] Leontidis, V., Chen, J., Baldas, L., and Colin, S., Numerical Design of a Knudsen Pump With Curved Channels Operating in the Slip Flow Regime, *Heat Mass Transfer*, vol. 50, pp. 1065–1080, 2014.

[8] Naris, S., and Valougeorgis, D., Gas Flow in a Grooved Channel Due to Pressure and Temperature Gradients, *Proc. ICNMMM2006-96225*, June 19–21, 2006, ASME, New York, NY, 2006.

[9] Masters, N. D., and Ye, W., Octant Flux Splitting Information Preservation DSMC Method for Thermally Driven Flows, *Journal of Computational Physics*, vol. 226, no. 2, pp. 2044–2062, 2007.

[10] Huang, J., C., Xu, K., and Yu, P., A Unified Gas-Kinetic Scheme for Continuum and Rarefied Flows III: Microflow Simulations, *Communications in Computational Physics*, vol. 14, no. 5, pp. 1147–1173, 2013.

[11] Aoki, K., Takata, S., and Aikawa, H., A Rarefied Gas Flow Caused by a Discontinuous Wall Temperature, *Physics of Fluids*, vol. 13, pp. 2645–2661, 2001.

[12] Sone, Y., Boundary Temperature Effect in a Highly Rarefied Gas, *Physics of Fluids*, vol. 28, pp. 419–420, 1985.

[13] Sone, Y., Comment on "Heat Transfer in Vacuum Packaged Microelectromechanical System Devices" [*Phys. Fluids* 20, 017103 (2008)], *Physics of Fluids*, vol.. 21, no. 11, pp. 119101–119102, 2009.

[14] Rana, A., Torrilhon, M., and Struchtrup, H., Heat Transfer in Micro Devices Packaged in Partial Vacuum, *Journal of Physics: Conference Series*, vol. 362, p. 012034, 2012.

[15] Vargas, M., Tatsios, G., Valougeorgis, D., and Stefanov, S. K., Rarefied Gas Flow in a Rectangular Enclosure Induced by Non-Isothermal Walls, *Physics of Fluids*, vol. 26, no. 5, pp. 057101, 2014.

[16] Sone, Y., *Kinetic Theory and Fluid Dynamics*, Birkhäuser, Boston, MA, 2002.

[17] Struchtrup, H., and Taheri, P., Macroscopic Transport Models for Rarefied Gas Flows: A Brief Review, *IMA Journal of Applied Mathematics*, vol. 76, no. 5, pp. 672–697, 2011.

[18] Cercignani, C., *The Boltzmann Equation and Its Applications*, Springer, New York, NY, 1988.

[19] Bird, G. A., *Molecular Gas Dynamics and the Direct Simulation of Gas Flows*, Clarendon, Oxford, UK, 1994.

[20] Rana, S. A., Mohammadzadeh, A., and Struchtrup, H., A Numerical Study of the Heat Transfer Through a Rarefied Gas Confined in a Microcavity, *Continuum Mechanics and Thermodynamics*, vol. 27, no. 3, pp. 433–446, 2015.

[21] Shakhov, E. M., Generalization of the Krook Kinetic Relaxation Equation, *Fluid Dynamics*, vol. 3, no. 5, pp. 142–145, 1968.

[22] Shakhov, E. M., Kinetic Model Equations and Numerical Results, *in Proceedings of 14th International Symposium on Rarefied Gas Dynamics*, University of Tokyo Press, Toko, Japan, pp. 137–148, 1984.

[23] Sharipov, F., and Seleznev, V., Data on Internal Rarefied Gas Flows, *Journal of Physical and Chemical Reference Data*, vol. 27, no. 3, pp. 657–706, 1998.

[24] Titarev, V. A., Dumbser, M., and Utyuzhnikov, S. V., Construction and Comparison of Parallel Implicit Kinetic Solvers in Three Spatial Dimensions, *Journal of Computational Physics*, vol. 256, pp. 17–33, 2014.

[25] Pantazis, S., and Valougeorgis, D., Non-Linear Heat Transfer Through Rarefied Gases Between Coaxial Cylindrical Surfaces at Different Temperatures, *European Journal of Mechanics B/Fluids*, vol. 29, pp. 494–509, 2010.

[26] Sharipov, F., Benchmark Problems in Rarefied Gas Dynamics, *Vacuum*, vol. 86, pp. 697–1700, 2012.

[27] Aristov, V. V., Shakhov, E. M., Titarev, V. A., and Zabelok, S. A., Comparative Study for Rarefied Gas Flow Into Vacuum Through a Short Circular Pipe, *Vacuum*, vol. 103, pp. 5–8, 2014.

[28] Misdanitis, S., Pantazis, S., and Valougeorgis, D., Pressure Driven Rarefied Gas Flow Through a Slit and an Orifice, *Vacuum*, vol. 86, no. 11, pp. 1701–1708, 2012.

[29] Pantazis, S., Naris, S., Tantos, C., Valougeorgis, D., Andre, J., Millet, F., and Perin. J. P., Nonlinear Vacuum Gas Flow Through a Short Tube Due to Pressure and Temperature Gradients, *Fusion Engineering and Design*, vol. 88, no. 9–10, pp. 2384–2387, 2013.

Giorgos Tatsios is a Ph.D. student at the Mechanical Engineering Department of the University of Thessaly, Volos, Greece. He obtained a diploma in mechanical engineering from the University of Thessaly in 2014. His research is focused on kinetic theory of gases with application in rarefied gas flows.

Manuel H. Vargas is a researcher in the field of rarefied gas dynamics who graduated as chemical engineer in 2005 from the University of Santiago de Compostela. In 2013 he defended succesfully his Ph.D. in mathematical modeling and application of mathematics at the Institute of Mechanics of the Bulgarian Academy of Sciences after receiving a Marie Curie Fellowship. In 2013 he joined the Department of Mechanical Engineering of the University of Thessaly as a postdoctoral researcher. His research contributions are in the field of Monte Carlo simulation method and its applications to rarefied gas dynamics and microfluidic problems.

Stefan K. Stefanov is a professor in mathematical modeling and application of mathematics at the Institute of Mechanics, Bulgarian Academy of Sciences. He received his Ph.D. in fluid mechanics in 1987 and second scientific degree doctor of sciences in mathematical modeling and applications of mathematics in 2011. From 2000 to 2010 he was head of the department for modeling of complex and multiphase flows. Currently he is a deputy head of the Department of Mathematical Modeling and Numerical Simulations. His research contributions are in the field of Monte Carlo simulation method and its applications to rarefied gas dynamics and microfluidic problems.

Dimitris Valougeorgis is a professor in the Department of Mechanical Engineering of the University of Thessaly in Volos, Greece. He obtained a diploma in mechanical engineering from the Aristotelion University of Thessaloniki, Greece, in 1980 and M.S. and Ph.D. degrees in mechanical engineering from the Virginia Polytechnic Institute and State University, USA, in 1982 and 1985, respectively. His research is in kinetic theory of gases, rarefied gas dynamics, and nonequilibrium transport phenomena. He has published about 65 articles in journals and more than 100 articles in proceedings of conferences. He has been in the organization and scientific committees of several conferences and workshops in gas microflows and vacuum gas dynamics.